Kinetic Studies of Chromium (VI) Binding to Carboxylic Acid- and Methyl Ester-Functionalized Silica/Water Interfaces Important in Geochemistry

Hind A. Al-Abadleh, Amanda L. Mifflin, Michael J. Musorrafiti, and Franz M. Geiger*

Department of Chemistry, Northwestern University, 2145 Sheridan Road, Evanston, Illinois 60208

Received: June 6, 2005; In Final Form: July 7, 2005

Real-time kinetic measurements of hexavalent chromium binding to fused silica surfaces functionalized with carboxylic acid and methyl ester terminal groups are performed in situ using resonantly enhanced surface second harmonic generation (SHG) at pH 7 and 300 K. These functional groups were chosen because of their high abundance in humic acids and related biopolymers. Kinetic measurements are conducted in the submonolayer regime using chromate solution concentrations ranging from 1×10^{-6} to 2×10^{-5} M. The adsorption rates were analyzed using the standard Langmuir model and the Frumkin−Fowler−Guggenheim model. The desorption kinetics are consistent with a first-order process. These results indicate that hexavalent chromium mobility in carboxylic acid- and ester-rich soil environments increases with decreasing chromate concentrations. Based on the measured half-lives of the adsorbed Cr(VI) species, remobilization of bound hexavalent chromium due to natural or anthropogenic events that lower the chromate concentration in the aqueous phase can occur within minutes.

I. Introduction

The fate and mobility of trace metal pollutants in soil environments can be controlled by processes occurring at mineral/water interfaces.[1,2] Biosurfactants and biopolymers are important in geochemical processes because of their ability to adsorb to mineral surfaces, where they can sequester metal pollutants out of the aqueous phase.[1,3−7] Biopolymers such as humic acids are rich in polar functional groups such as carboxylic acids, esters, di- or trihydroxyphenols, quinones, and α-hydroxy carboxylic acids.[2] In this work, we investigate the interaction kinetics between surface-bound carboxylic acid and ester groups and Cr(VI), one of the key metals on the EPA pollutant priority list.[8]

Hexavalent chromium, one of the two stable forms of chromium in aqueous solutions under neutral pH,[9] is carcinogenic, toxic, and highly mobile in most soil environments.[10−24] At polluted sites, chromium concentrations can be several orders of magnitude higher than the maximum allowable limit for total chromium in groundwater in the US, which is 2×10^{-6} M.[25] To improve our understanding of chromium mobility in the environment, intense research has focused on the interaction of chromate with minerals and natural organic matter.[26−39] For example, adsorption isotherms obtained from batch studies[38,40−42] yield important information for assessing the magnitude of these interactions, such as free adsorption energies, equilibrium binding constants, and saturation surface coverages of Cr(VI). These parameters can be used for predicting Cr(VI) mobility in soils by calculating chromate retardation factors[43−45] from solid−liquid partition coefficients. However, the variety of organic functional groups present in batch samples can lead to convoluted contributions of the individual interaction energies in the measured overall adsorption equilibrium constant. This is particularly problematic when the interaction of Cr(VI) with the various functional groups is governed by the same process, such as hydrogen bonding. Furthermore, tracking the chromate binding kinetics directly at the aqueous/solid interface represents an experimental challenge, especially when considering that adsorption and desorption rate measurements require real-time detection of surface coverages below saturation.[46]

In addition to batch studies, XAFS and EXAFS are extremely useful for characterizing sorption products and speciation with surface specificity and for analyzing the first and second solvation sphere structure,[47−50] adsorbate geometries,[26,28,51,52] and the oxidation state of adsorbed chromium.[53] However, some chromium species, including Cr(VI), can be reduced in the presence of X-rays, making the elucidation of oxidation states via X-ray spectroscopy challenging.[26] In general, surface-specific approaches for studying chromium interaction with geosorbents are limited by low sensitivities. Due to the nonlinear relationship between aqueous phase concentration and surface coverage for small aqueous phase concentrations,[46] the application of kinetic, thermodynamic, mechanistic, and structural data from experiments that use high concentrations to environmentally representative chromate concentration conditions is problematic. Thus, in the context of environmentally relevant chromium concentrations, the understanding of chromium binding to various substrates remains qualitative.[28,41,42,52,54−56]

In this work, we use functionalized organic surfaces in a reductionist model study aimed at understanding how hexavalent chromium binds to organic adlayers at mineral/water interfaces under dynamic, off-equilibrium conditions. Specifically, we track the interaction of aqueous phase Cr(VI) with carboxylic acid- and methyl ester functional groups at silica/water interfaces. By working under neutral pH conditions and in the absence of redox-active metal ions, this model system allows us to focus specifically on the binding events while chromate interacts with the surface-bound organic functional groups. By functionalizing the solid substrate surfaces with organosilanes that contain the specific organic groups under investigation, we avoid chelating interactions between dissolved chromate and dissolved organic species in the aqueous phase. Further, we

* To whom correspondence should be addressed. E-mail: geigerf@chem.northwestern.edu.

10.1021/jp053006p CCC: $30.25
Published on Web 08/11/2005

circumvent issues arising from the competitive coadsorption of the dissolved species. Our strategy for generating organic adlayers that simulate biosurfactants and related surface-active species allows for high control over the chemistry, structure, and order of the surface-bound environmentally relevant molecules.

A description of the synthetic procedures for preparing the carboxylic acid- and the methyl ester-terminated adlayers and their characterization is given elsewhere.[57−59] Most importantly for this work, we found the carboxylic acid-functionalized surfaces to be essentially neutral at pH 7[59] and that chromate adsorption to the acid- and ester-functionalized surfaces leads to S-shaped adsorption isotherms.[60] This adsorption behavior is consistent with the Frumkin−Fowler−Guggenheim (FFG) model,[61] which predicts a coverage-dependent binding constant of $K_{ads}\exp(g\theta)$ that can be attributed to stabilizing lateral adsorbate−adsorbate interactions among the adsorbed Cr(VI) species. The FFG model allowed for the parametrization of chromate retardation factors in silica-rich soils whose particle surfaces contain organic adlayers rich in carboxylic acid and methyl ester groups. We found that under equilibrium conditions, chromate would move up to three times slower than would be predicted by the simple, albeit widely used, Kd transport model.[43−45] Here, we investigate whether these results, which were obtained under equilibrium conditions, also hold under the dynamic conditions most commonly found in soil environments.[62]

II. Experimental Section

Real-time kinetic measurements of chromate binding to the carboxylic acid- and methyl ester-functionalized silica/water interfaces were carried out in the submonolayer surface coverage regime using resonantly enhanced surface second harmonic generation (SHG).[63−65] Nonlinear optical spectroscopies are well-established surface science techniques and have been applied to environmentally relevant surfaces and buried interfaces.[57,59,60,63,66−84] The experiments were conducted using the dual pump-flow and laser systems described in detail previously.[83,84] Briefly, the flat side of the 1 in. diameter fused quartz hemispherical lens (ISP Optics) was functionalized with the organosilane under investigation and then clamped leak-tight to a custom-built Teflon liquid flow cell via a Viton O-ring. The aqueous chromate solution (K_2CrO_4, ICN Biomedicals) and water (Millipore, 18 MΩ) maintained at pH 7 were pumped across the interface using flow-controlled peristaltic pumps (Fisher). The bulk chromate concentration was measured using UV−vis spectroscopy (Ocean Optics) simultaneously with the SHG signal. The flow rate was measured after the mixing point of the potassium chromate solution with water and before the flow cell using a glass flow meter (Fisher). The experiments were carried out under controlled-flow conditions while maintaining a total flow rate of 0.52(5) mL/s. The concentration of the chromate solution in a typical experiment ranged between 1×10^{-6} and 2.2×10^{-5} M, corresponding to environmentally representative concentrations and submonolayer coverages. After completing each adsorption/desorption cycle, the concentration of the chromate solution in the reservoir was increased, and the experiment was repeated. The cumulative exposure time of the interfaces to chromate was limited to less than 35 min per sample to avoid surface deterioration.[60]

Details about the laser system used in these experiments are provided elsewhere.[83,84] Briefly, the system consists of a Ti:sapphire laser (kHz, 120 fs, Hurricane, Spectra Physics) pumping an optical parametric amplifier (OPA-CF, Spectra Physics). The output light from the OPA at 580 nm was focused onto the aqueous/solid interfaces at an angle of about 60° and with a spot size approximately 50 μm in diameter. The SHG signal at 290 nm was collected using a single photon counting system after filtering signals from processes other than SHG via Schott filters and a monochromator. Typical input pulse energies are 3 μJ or less.

III. Second Harmonic Generation

The recorded SHG intensity, I_{SHG}, is related to the second-order susceptibility of the interface, $\chi^{(2)}_{int}$.[63−65] When the SHG E-field, E_{SHG}, is resonantly enhanced, as in the case of adsorbed Cr(VI), $\chi^{(2)}_{int}$ consists of a nonresonant and a resonant contribution, $\chi^{(2)}_{NR}$ and $\chi^{(2)}_{R}$, respectively. With $\chi^{(2)}_{NR}$ being real, these two contributions are linked by the difference in their respective phases, $\Delta\phi$, as shown in eq 1

$$\sqrt{I_{SHG}} = E_{SHG} \propto \sqrt{|\chi^{(2)}_{NR} + \chi^{(2)}_{R} e^{i\Delta\phi}|^2} \qquad (1)$$

The resonant contribution to the second-order susceptibility, $\chi^{(2)}_{R}$, can be modeled as the product of the number of molecules adsorbed on the surface, N, and the molecular hyperpolarizability, $\alpha^{(2)}$, averaged over all molecular orientations, according to eq 2

$$\chi^{(2)}_{R} = N\langle\alpha^{(2)}\rangle \qquad (2)$$

Equations 1 and 2 show that SHG can be used to perform thermodynamic and kinetic studies of heterogeneous processes by monitoring the concentration- and the time-dependence of the SHG E-field. Equation 1 can be simplified using the Euler identity to[85]

$$\frac{|\vec{E}_{2\omega}|}{|\vec{E}_{\omega}|^2} \propto \sqrt{(\chi^{(2)}_{NR})^2 + (\chi^{(2)}_{R})^2 + 2\chi^{(2)}_{NR}\chi^{(2)}_{R}\cos(\Delta\phi)} \qquad (3)$$

Thus, to extract values of $\chi^{(2)}_{R}$ from eq 1, it is important to know the phase difference, $\Delta\phi$, of the second-order susceptibility contributions. As we will demonstrate briefly for the case of a first-order desorption process, taking this phase difference into account is important in kinetic studies. For a first-order decay process,[86] $N = \theta_0 N_{ML}\exp(-kt)$, where k is the desorption rate constant and θ_0 is the initial relative surface coverage before desorption is initiated. Substituting this expression and eq 2 into eq 3 results in the following relation:

$$\frac{|\vec{E}_{2\omega}|}{|\vec{E}_{\omega}|^2} \propto \sqrt{(\chi^{(2)}_{NR})^2 + {\theta_0}^2 {N_{ML}}^2 e^{-2kt}\langle\alpha^{(2)}\rangle^2 + 2\chi^{(2)}_{NR}\theta_0 N_{ML} e^{-kt}\langle\alpha^{(2)}\rangle\cos(\Delta\phi)} \qquad (4)$$

Figure 1A shows a plot of eq 4 as a function of time (in arbitrary units) and phase difference (in degrees) using the following parameters (in arbitrary units): $\theta_o = 1$ (i.e., monolayer coverage), a rate constant, k, of 2 (in arbitrary units), $\chi^{(2)}_{NR} = 50$ and $N_{ML}\langle\alpha^{(2)}\rangle = 100$. Cross sections of constant $\Delta\phi$ represent the kinetic traces for that particular phase difference. Figure 1A shows that the exponential decay of the SHG E-field with time does depend on the phase difference between the resonant and the nonresonant $\chi^{(2)}$ contributions. The effect is most dramatic for phase differences approaching 180°, where the SHG

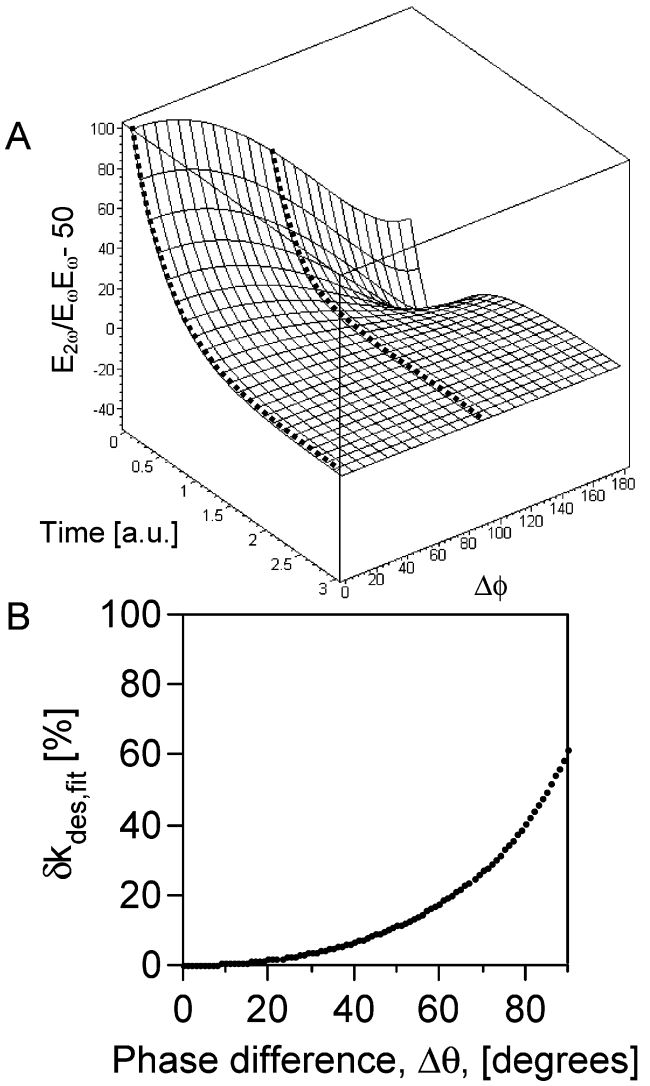

Figure 1. (A) Calculated SHG E-field response vs time for a first-order desorption process as a function of phase difference, $\Delta\phi$, between the resonant and the nonresonant $\chi^{(2)}$ contributions. Desorption traces calculated for a zero and a ninety degree phase difference are indicated by the dashed lines. (B) Relative error in the first-order desorption rate constant due to uncertainties in $\Delta\phi$ assuming a zero degree phase difference. See text for details.

E-field temporarily decreases to levels below the nonresonant background level. However, for phase differences ranging between 0° and 90°, the SHG E-field will decay monotonically in time, which is what is observed in the experimental SHG vs time traces.

Clearly, if the phase difference of the second-order susceptibility contributions is not known, rate constants cannot be determined. One thus assumes a phase difference and applies eq 4 to the experimental time traces. However, assuming a phase difference will clearly result in uncertainties in the rate constants. We assessed this uncertainty by fitting time traces from Figure 1A that correspond to various phase differences to eq 4 while holding the phase difference at zero in each fit. The results are shown in Figure 1B, in which the percent deviation of the rate constants from the original rate constant ($k = 2$) is plotted against phase differences between 0° and 90°. At monolayer coverage, the deviations in the rate constants can be as high as 60%. We thus analyzed the measured SHG vs time traces with a phase difference of 0° and 90° to assess this possible uncertainty in our kinetic measurements. For this analysis, we

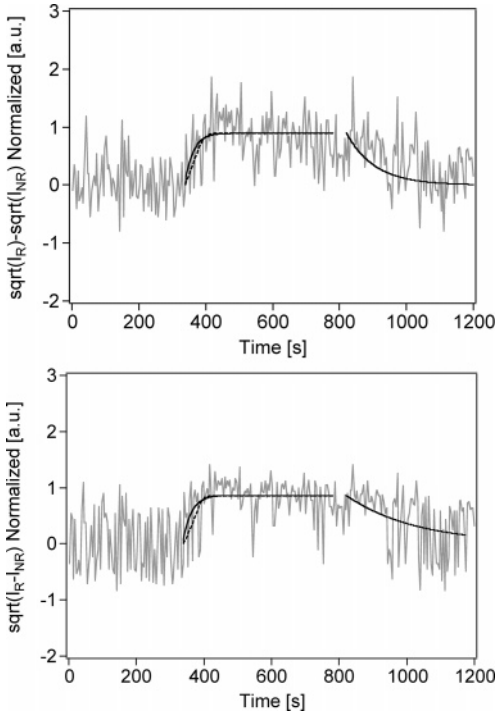

Figure 2. Time trace of the SHG E-field at $\lambda_{SHG} = 290$ nm for chromate adsorption on an acid-functionalized silica/water interface at pH 7 and 300 K ($[CrO_4^{2-}] = 2.1 \times 10^{-5}$ M). SHG background subtraction was performed in accordance with a phase difference, $\Delta\phi = 0°$ (top) $\Delta\phi = 90°$ (bottom). Data were normalized to the maximum net SHG E-field obtained in the monolayer regime. The solid line in the adsorption portion is a fit to the data according to eq 8, and the dashed line is the solution of eq 12. The solid line in the desorption portion is the first-order desorption fit according to eq 10. See text for details.

applied the following background subtraction methods to obtain the resonant $\chi^{(2)}$ contribution from eq 3: in the case of $\Delta\phi = 0°$, $\chi_R^{(2)}$ is related to the SHG intensity via eq 5

$$\chi_R^{(2)} = \sqrt{I_R} - \sqrt{I_{NR}} \tag{5}$$

whereas for $\Delta\phi = 90°$, $\chi_R^{(2)}$ is related to the SHG intensity via eq 6

$$\chi_R^{(2)} = \sqrt{I_R - I_{NR}} \tag{6}$$

IV. Results and Discussion

Figure 2 shows a representative SHG time trace for chromate (2.1×10^{-5} M) binding to the acid-functionalized silica/water interface. The top and bottom panels show the resulting SHG vs time trace assuming $\Delta\phi = 0°$ and 90°, respectively, normalized to the maximum relative surface coverage obtained for similar time traces in the monolayer regime. The data were smoothed by averaging every three consecutive data points in raw SHG counts and time. During the chromate adsorption process, an increase in the SHG E-field is observed. This increase is consistent with our previous observation of SHG resonance enhancement in the presence of adsorbed Cr(VI) at the fused quartz/water interface.[83,84] Upon reaching equilibrium between adsorbed Cr(VI) and chromate in solution, the SHG E-field levels off. Based on our adsorption isotherm measurements,[60] the normalized surface coverage reached in the experiment shown in Figure 2 is 80(8)% of a monolayer. When the aqueous phase chromate solution is replaced with plain water at the same pH, the SHG E-field decreases to its background

level, consistent with chromate desorption from the surface. Chromate binding to the ester-functionalized silica/water interface results in similar SHG vs time traces.[60]

In the following section, we analyze the kinetic data for chromate adsorption using simple Langmuir adsorption kinetics, in which the equilibrium constant is independent of surface coverage.[87] Then, we analyze the desorption portion of the SHG time traces using a first-order desorption kinetics model. Zero-order kinetics could play a role here as well. The times required for reaching 50% of the steady-state signal levels during the adsorption and desorption portions of the SHG E-field vs time traces range between 30 and 90 s for adsorption and desorption. Within experimental error, these half-lives do not depend on the chromate concentration used, suggesting that the adsorption and desorption processes are associated with first order kinetics. Finally, we apply the results from the desorption rate measurements in an adsorption model that takes into account a coverage-dependent equilibrium constant, i.e., the FFG model.[61]

A. Chromate Adsorption: Langmuir Model Kinetics. The kinetic data for chromate binding to the functionalized silica/water interfaces were analyzed using the simple Langmuir model with a first-order desorption rate.[87] In this scenario, the adsorption rate for the equilibrium process Cr(VI) (aq) + surface site ↔ Cr(VI) (ad) is expressed as

$$\frac{d\theta}{dt} = k_{ads}C_{bulk}(1-\theta) - k_{des}\theta \tag{7}$$

where C_{bulk} is the chromate concentration in the bulk aqueous phase, θ is the Cr(VI) surface coverage, and k_{ads} and k_{des} are the adsorption and the desorption rate constants, respectively. After integration, eq 7 yields

$$\theta = b(1 - e^{-r_{obs}t}) \tag{8}$$

Here r_{obs} is the observed rate for chromate binding, which is given by

$$r_{obs} = k_{ads}C_{bulk} + k_{des} \tag{9}$$

In eq 8, b is the relative steady-state surface coverage, referenced to the monolayer surface coverages obtained from the adsorption isotherm measurements.[60] Equation 8 was used to fit the SHG vs time traces assuming a $\Delta\phi = 0°$ and 90° for a range of chromate concentrations in the submonlayer regime. The solid black lines in Figure 2 show a representative fit to the adsorption portion of the SHG vs time trace for chromate binding to the acid-functionalized silica/water interface.

Each chromate concentration yields a value for r_{obs}, as shown in Figure 3 for the acid-functionalized (A) and the ester-functionalized (B) silica/water interface. The solid and dashed lines are fits of eq 9 to the data, and the results are summarized in Table 1 under the heading "Langmuir model". There are two main points that can be extracted from this simple analysis. First, the scatter in Figure 3 is quite high, which results in high uncertainties in the adsorption and desorption rate constants derived from the simple Langmuir model. Second, within experimental error, the phase difference does not appear to have a significant effect on the adsorption and desorption rate constants, as shown in Table 1. This is consistent with the discussion presented in section II.

In contrast to the simple Langmuir model, the FFG framework includes lateral adsorbate−adsorbate interactions and predicts a coverage-dependent Cr(VI) binding constant of the form $K(\theta) = K_{ads}\exp(g\theta)$.[61] Since the binding constant is given by the ratio of the adsorption and the desorption rate constants,[88] the kinetics of chromate adsorption and/or desorption could be modulated by the chromate surface coverage. This, in turn, could have significant consequences for chromium mobility in the environment. Therefore, we will explore the Cr(VI) coverage-dependence of the adsorption and desorption kinetics, and start with the latter in the following section.

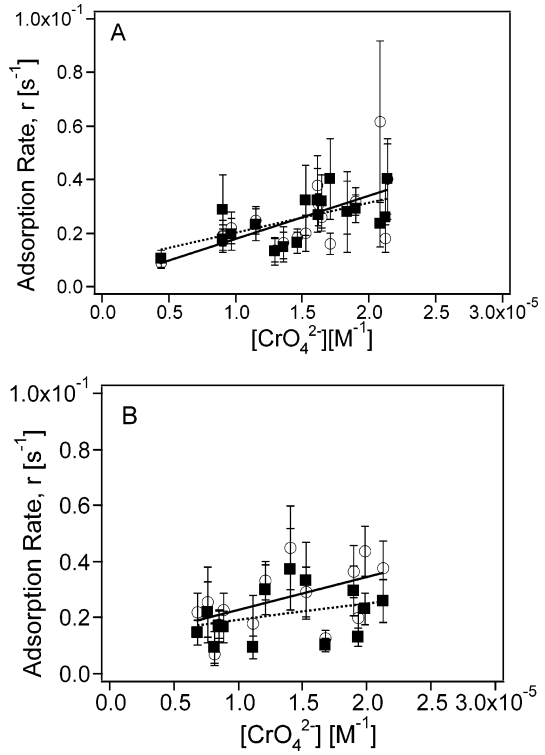

Figure 3. Chromate adsorption rates measured as a function of chromate concentration for (A) acid-functionalized and (B) ester-functionalized silica/water interfaces at pH 7 and 300 K. The solid ($\Delta\phi = 90°$) and dashed ($\Delta\phi = 0°$) lines are fits to the data according to eq 9. Two data sets are shown in each panel that corresponds to data points extracted from a phase difference of $\Delta\phi = 0°$ (filled squares) $\Delta\phi = 90°$ (empty circles).

B. Cr(VI) Desorption Kinetics. The kinetics of chromate desorption from the acid- and the ester-functionalized silica/water interfaces were measured as a function of Cr(VI) surface coverage in the submonolayer regime and were analyzed using a first-order desorption kinetic model of the form[84]

$$\theta = b(e^{-k_{des}t}) \tag{10}$$

Here, b is again the relative surface coverage, referenced to the monolayer surface coverages obtained from the adsorption isotherm measurements,[60] before the chromate solution in the bulk aqueous phase is replaced by water. The solid lines in the desorption portion of Figure 2 show a representative fit of eq 10 to the SHG vs time traces for chromate desorbing from the acid-functionalized silica/water interface. The dependence of the desorption rate constant, k_{des}, on the Cr(VI) surface coverage is plotted in Figure 4 for (A) the acid-functionalized and (B) the ester-functionalized silica/water interface. Within the noise, the different background subtraction methods have no appreciable effect on the desorption parameters.

Figure 4 shows that, within experimental error, the relative desorption rate constant appears to be independent of Cr(VI) surface coverage and thus bulk chromate solution concentration. This is expected since desorption rate constants should not depend on the surface coverage of the desorbing species.[61,88,89]

TABLE 1: Summary of Kinetic Parameters Obtained from Fitting the SHG vs Time Traces with the Standard Langmuir Adsorption Model, a First-Order Desorption Model, and the FFG-Modified Langmuir Model

	Langmuir model $\Delta\phi = 0°$		Langmuir model $\Delta\phi = 90°$		first-order desorption model $\langle k_{des}\rangle$[s^{-1}]		FFG model[a]
surface	k_{ads} [s^{-1} M^{-1}]	k_{des} [s^{-1}]	k_{ads} [s^{-1} M^{-1}]	k_{des} [s^{-1}]	$\Delta\phi = 0°$	$\Delta\phi = 90°$	k_{ads} [s^{-1} M^{-1}]
acid	1128(365)	0.008(6)	1615(515)	0.002(8)	0.012(4)	0.011(6)	250(50)
ester	587(496)	0.013(7)	1180(554)	0.011(8)	0.017(5)	0.013(4)	660(180)

[a] Average of the kinetic results obtained from analyzing the SHG vs time traces with the FFG model for the cases of $\Delta\phi = 0°$ and $\Delta\phi = 90°$.

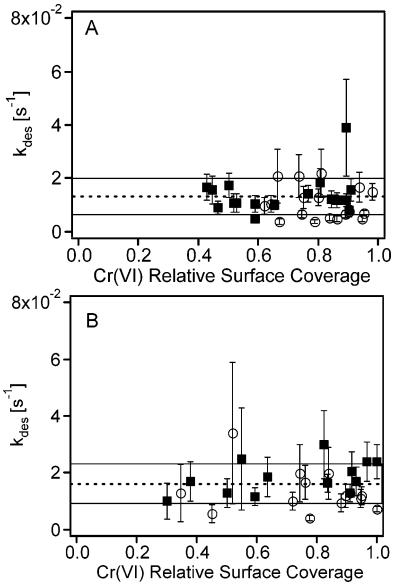

Figure 4. Dependence of the measured desorption rate constant on Cr(VI) surface coverage for chromate desorption from (A) the acid-functionalized, and (B) the ester-functionalized silica/water interfaces, respectively. Two data sets are shown in each panel that correspond to data points extracted using a phase difference of $\Delta\phi = 0°$ (filled squares) and $\Delta\phi = 90°$ (empty circles). In each plot, the dashed line represents the average value of k_{des} for both phase differences. The solid lines represent the upper and lower limits.

The dashed lines shown in Figure 4 represent the average k_{des} value, for (A) the acid- and (B) the ester-functionalized silica/water interfaces, respectively, their upper and lower error limits being indicated by the black lines. These desorption rate constants are listed in Table 1 under the heading "first-order desorption model". It can be seen that the desorption rate constants obtained from the desorption portion of the kinetic traces are consistent with the ones derived from the adsorption rate measurements, however, they are associated with smaller uncertainties.

C. Chromate Adsorption: FFG Model Kinetics. Provided that the desorption rate constant k_{des} is coverage-independent, which we verified in the previous section, the FFG-parametrized adsorption rate constant k'_{ads} can be now rewritten as $k'_{ads} = k_{des}K_{ads}\exp(g\theta)$. The unparametrized adsorption rate constant, k_{ads}, is then given by $k_{ads} = k'_{ads}/\exp(g\theta) = k_{des}K_{ads}$. Substituting the FFG-parametrized k'_{ads} expression into the adsorption rate equation of the simple Langmuir model, eq 7, one obtains

$$\frac{d\theta}{dt} = k_{des}K_{ads}e^{g\theta}C_{bulk}(1-\theta) - k_{des}\theta \qquad (11)$$

Equation 11 can be solved numerically for each chromate concentration. In this expression, k_{des} is obtained from fitting the desorption portion of the time trace to the first-order desorption model, and K_{ads} and g are obtained from fitting the FFG model to the adsorption isotherm data obtained for the acid- and the ester-functionalized surfaces.[60] A simple MATHCAD program was written to numerically solve the differential equation in the adsorption regime of the SHG vs time traces, according to

$$\frac{d\theta}{dt} = k_{des}K_{ads}e^{g\theta}C_{bulk}(b-\theta) - k_{des}\theta + k_{des}b \qquad (12)$$

where b is again the relative normalized surface coverage reached at equilibrium. The initial conditions are chosen such that, at zero time, the surface coverage, θ, equals zero. An example fit is shown in Figure 2, where the dashed line is the result of numerically solving eq 12 for chromate adsorption on an acid-functionalized silica/water interface using the following input parameters: $k_{des} = 0.012$ s^{-1}, $K_{ads} = 1.98 \times 10^4$ M^{-1}, $g = 3.2$, and $C_{bulk} = 2.1 \times 10^{-5}$ M. The relative normalized equilibrium surface coverage, b, was 0.89, as determined from our adsorption isotherm measurements.[60] These parameters generate an adsorption trace (dashed line) that is slightly shallower and more linear at early times than the simple Langmuir model (solid line) and suggest that thermodynamic parameters derived from equilibrium adsorption isotherm measurements may be directly transferable to the kinetic rate expressions. With these parameters, the adsorption rate constant, k_{ads}, would be 2.4×10^2 M^{-1} s^{-1} for this particular experiment.

To extract the adsorption rate constants from fits of eq 8 to the kinetic data without using the K_{ads} obtained from the equilibrium adsorption isotherm measurements,[60] we introduced a fitting parameter, A, that replaces the constants k_{des} and K_{ads} in the first term of eq 11. In this case, A is the adsorption rate constant k_{ads}. The exponential g term is still included in the fits. We numerically solved eq 12 while varying the value of A for a given adsorption time trace until the best fit to the adsorption portion of the SHG vs time trace was obtained. The results are shown in Figure 5 for both the acid- and ester-functionalized surfaces, where the empty squares represent the A parameters obtained from the best fits to the kinetic traces. For comparison, the filled circles represent the k_{ads} values, given by k_{des} multiplied by K_{ads}. We find that the A values, obtained from the kinetic fits, are in good agreement with the product of the desorption rate constant, k_{des}, and the equilibrium constant for adsorption, K_{ads}. Finally, the A and k_{ads} parameters appear independent of chromate concentration within experimental error. Again, the two background subtraction schemes (corresponding to phase differences of 0° and 90°) do not appear to significantly affect the kinetic parameters.

Our analysis of the adsorption and desorption traces is consistent with first-order adsorption and desorption kinetics, in which the adsorption process is modulated by the exponential Boltzmann term stemming from the FFG model (viz eq 11). Within this framework, plotting the FFG-parametrized adsorption rate constant, k'_{ads}, as a function of Cr(VI) surface coverage should lead to an exponential increase of k'_{ads} with Cr(VI) surface coverage. Figure 6, panels A and B, shows that this is indeed the case for the acid- and the ester-functionalized surfaces, respectively. The solid line through the data is a test for self-consistency of the above relation $k'_{ads} = k_{des}K_{ads}\exp(g\theta)$, in which we used the average value of k_{des} obtained for each interface as a function of surface coverage (Figure 4).

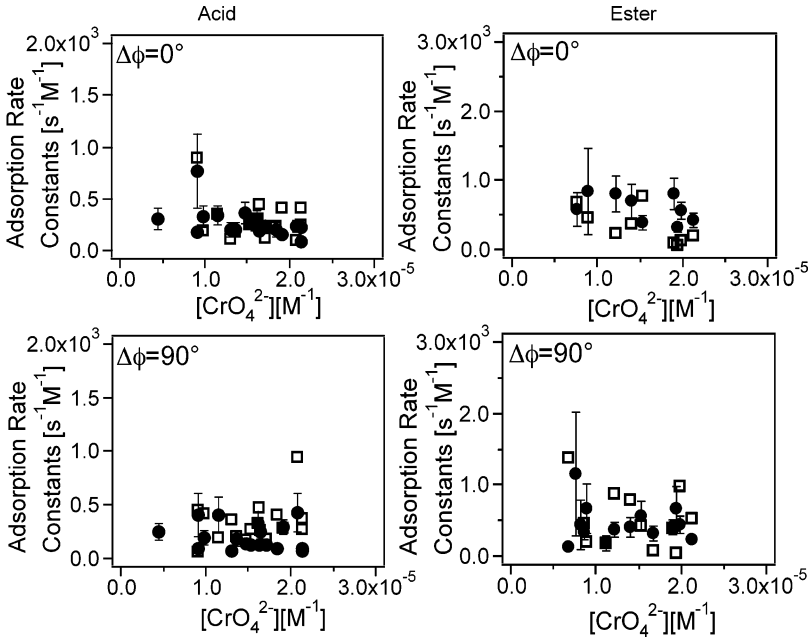

Figure 5. Dependence of the *A* parameter (empty squares) and k_{ads} (filled circles) on chromate concentration for chromate adsorption on the acid- (left panel) and ester-functionalized (right panel) silica/water interfaces at pH 7 and 300 K. Values of k_{ads} are calculated according to the relation $k_{ads} = k_{des}K_{ads}$ for each chromate concentration, and *A* values are obtained from the best fit to the adsorption portion of the SHG time traces by numerically solving eq 8. Phase differences for the background subtraction are $\Delta\phi = 0°$ (top) and $\Delta\phi = 90°$ (bottom). See text for details.

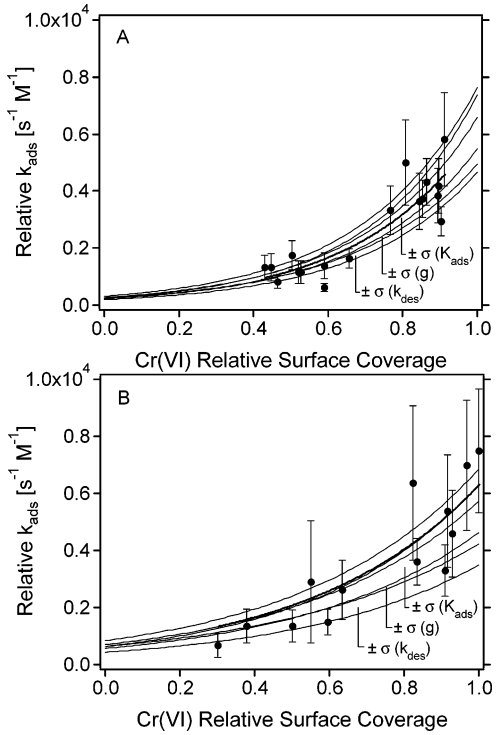

Figure 6. Dependence of the FFG-parametrized adsorption rate constant, k'_{ads}, on Cr(VI) surface coverage on (A) acid-functionalized, and (B) ester-functionalized silica/water interfaces at pH 7 and 300 K. Values of k_{ads} are calculated according to the relation $k'_{ads} = k_{des}K_{ads}\exp(g\theta)$ using experimentally determined values for k_{des}, K_{ads}, g, and θ. The thick dashed lines through the data are a test for self-consistency of the model using k_{des} values averaged over surface coverage as shown in Figure 4. The thin solid lines represent the errors associated with k_{ads} values from the 1σ standard deviation in k_{des}, K_{ads}, and g, calculated for chromate adsorption to the (A) the acid-functionalized and (B) the ester-functionalized silica/water interface, respectively. See text for details.

D. Error and Sensitivity Analysis. The uncertainty in the calculated FFG parameterized adsorption rate constants, k'_{ads}, stems from the uncertainty in each of the parameters used to calculate k'_{ads}, namely k_{des}, K_{ads}, and g. Figure 6 shows the errors in the k'_{ads} values that originate from the uncertainties in each of the above parameters calculated for chromate adsorption on (A) the acid-functionalized and (B) the ester-functionalized silica/water interfaces. The magnitude of the error in k'_{ads} is directly related to the width of the area calculated from the 1σ standard deviations associated with the average desorption rate constants. The uncertainties in k'_{ads} due to the uncertainties associated with K_{ads} and g are shown in Figure 6 as the thin solid lines. Clearly, the uncertainty in the desorption rate constant is the most important contributor to the uncertainty in the adsorption rate constant. A sensitivity analysis,[89] meant to quantify variations in the adsorption rates in eq 11 with the experimentally determined parameters g, K_{ads}, and k_{des}, also shows that the largest contribution to the uncertainty in the adsorption rate is due to the uncertainty in k_{des}.

E. Linking Kinetics and Thermodynamics. The data shown in Figure 6 can be extrapolated to the limit of zero surface coverage from which one can estimate K_{ads} values. For example, from Figure 6A for chromate binding to the acid-functionalized silica/water interface, k'_{ads} is 250(50) s^{-1} M^{-1} for $\theta = 0$. With an average desorption rate constant of 0.012(4) s^{-1}, one obtains an equilibrium constant of $2.1(8) \times 10^4$ M^{-1}. Using the molarity of water under standard conditions (55.5 M) as the reference state,[46] the free energy of adsorption for the zero surface coverage limit at 300 K is calculated to be 35(1) kJ/mol. For the ester-functionalized silica/water interface, k_{ads} is extrapolated to have a value of 660(180) s^{-1} M^{-1} for $\theta = 0$. With an average k_{des} of 0.017(5) s^{-1}, the resulting K_{ads} is $4(2) \times 10^4$ M^{-1}, and the free energy of adsorption at 300 K and in the zero coverage limit is found to be 36(1) kJ/mol. These values are in good agreement with the free energies of Cr(VI) binding to the acid- and ester-functionalized surfaces that we obtained from our previous adsorption isotherm measurements.[60] The finding that kinetic and thermodynamic measurements result in comparable equilibrium constants and free energies of adsorption for chromate binding to the various surfaces under investigation in

this work suggests that laboratory experiments carried out under equilibrium vs dynamic conditions are equivalent within the time frame of our kinetic measurements. Our measurements indicate, however, that the ability to detect submonolayer surface coverages is necessary for a detailed description of the contaminant-surface interaction events. This is found to be especially important when considering the FFG-parametrized adsorption rate constants, which exhibits its nonlinear dependence on Cr(VI) surface coverage in the submonolayer regime.

V. Possible Environmental Implications

Based on the kinetic results presented here, one can make estimates about hexavalent chromium mobility. One of the most commonly used models for assessing contaminant transport is the Kd model, which predicts the extent of contaminant transport, or the retardation, with respect to the free-flowing groundwater phase.[43−45] This model uses a binding parameter that is independent of the contaminant concentration. Our work shows that this model may not be applicable at all times for assessing the mobility of contaminants, specifically hexavalent chromium: the adsorption kinetics are consistent with an adsorption rate constant that is parametrized according to the Frumkin-Fowler-Guggenheim model. This would result in a dependence of the chromate adsorption kinetics on chromate concentration, with faster adsorption occurring at higher Cr(VI) surface coverages. The desorption rate constant is found to be independent of Cr(VI) coverage. This dependence of the chromium binding efficiency on chromium concentration in bulk solution would thus be controlled by the FFG-parametrized adsorption rate constant.

The rate constants derived from the present work and the equilibrium constants derived from our previous work[60] are valuable for assessing the mobility of hexavalent chromium in soil environments. The implications for the environmental fate of hexavalent chromium in carboxylic acid- and ester-rich, redox-inactive soil environments are clear: in the presence of surface-bound carboxylic acid and ester groups, low chromate concentrations will result in slow rates of Cr(VI) adsorption to aqueous/solid interfaces. Under those low concentration conditions, Cr(VI) will be more mobile than under high concentration conditions. This information can be included in chemical transport models for accurately predicting Cr(VI) mobility in organic-rich soil environments, and for assessing the fate of contaminants under varying contaminant concentration conditions.

Our findings may also have important consequences for Cr(VI) remediation strategies that are based on heterogeneous iron−chromium redox chemistry:[36,90,91] if the iron or iron (II) oxide surfaces are coated with biopolymers or humic acids, which is likely to be the case in aged semipermeable reactive barriers, the high mobility of hexavalent chromium that we observe on such functionalized surfaces at low chromate concentrations may not result in enough Cr(VI)-surface site interaction events for efficient Cr(VI) reduction. Likewise, this work shows that rain events, which would result in a temporary dilution of the chromate concentration in the aqueous phase, can quickly wash away the adsorbed Cr(VI): the first-order desorption rate constants reported here result in half-lives of 30−90 s, indicating that natural or anthropogenic events leading to drops in the chromate bulk phase concentrations can remobilize hexavalent chromium within minutes.

VI. Conclusions

In this work, we studied the kinetics of chromate adsorption and desorption from carboxylic acid- and ester-functionalized silica/water interfaces using resonantly enhanced surface second harmonic generation (SHG) at pH 7 and 300 K. Adsorption and desorption measurements were conducted in the submonolayer regime using chromate solution concentrations ranging from 1×10^{-6} to 2×10^{-5} M. First-order desorption rate kinetics are used to fit the desorption traces. Since our previous adsorption isotherm measurements are consistent with the Frumkin−Fowler−Guggenheim model, the adsorption rate measurements were analyzed with and without inclusion of a coverage-dependent Boltzmann factor in the adsorption rate expression. Our results are consistent with a parametrized adsorption rate constant that increases with Cr(VI) surface coverage. The environmental implication of this work is that the mobility of hexavalent chromium in redox-inactive, organic-rich soil environments is higher at low Cr(VI) concentrations than at high Cr(VI) concentrations. Further, remobilization of hexavalent chromium due to natural or anthropogenic events that lower the chromate concentration in the aqueous phase can occur within minutes.

Acknowledgment. The authors acknowledge fruitful conversations with Professor Garth Simpson (Purdue). We also gratefully acknowledge the donations and technical support of Spectra Physics and CVI Lasers. Financial support for this work was provided by the NSF (CAREER Award CHE-0348873), the ACS-PRF (Grant 38960-G5S), the Northwestern Institute for Environmental Catalysis (CHE-9810378 and DE-FG02-03-ER15457), and the Northwestern Nanoscale Science and Engineering Center (EEC-0118025).

References and Notes

(1) Stumm, W.; Morgan, J. J. *Aquatic Chemistry*, 3rd ed.; Wiley-Interscience: New York, 1996.

(2) Evangelou, V. P. *Environmental Soil and Water Chemistry*; John Wiley & Sons: New York, 1998.

(3) Brown, G. E.; Henrich, V. E.; Casey, W. H.; Clark, D. L.; Eggleston, C.; Felmy, A.; Goodman, D. W.; Gratzel, M.; Maciel, G.; McCarthy, M. I.; Nealson, K. H.; Sverjensky, D. A.; Toney, M. F.; Zachara, J. M. *Chem. Rev.* **1999**, *99*, 77.

(4) Brown, G. E. *Science* **2001**, *294*, 67.

(5) Warren, L. A.; Haack, E. A. *Earth-Sci. Rev.* **2001**, *54*, 261.

(6) Gustafsson, J. P.; Pechova, P. *Environ. Sci. Technol.* **2003**, *37*, 2767.

(7) Schwarzenbach, R. P.; Gschwend, P. M.; Imboden, D. M. *Environmental Organic Chemistry*, 2nd ed.; John Wiley and Sons: Hoboken, NJ, 2003.

(8) List of drinking water contaminants and MCLs; US Environmental Protection Agency, 2003; http://www.epa.gov/safewater/mcl.html.

(9) Sena, M. M.; Scarminio, I. S.; Collins, K. E.; Chollines, C. H. *Talanta* **2000**, *53*, 453.

(10) Katz, S. A.; Salem, H. *The Biological and Environmental Chemistry of Chromium*; VCH: New York, 1994.

(11) Nriagu, J. O.; Nieboer, E. *Chromium in the Natural and Human Environments*; John Wiley & Sons: New York, 1988.

(12) Goldman, L. R.; Lanphear, B. P. *Science* **1998**, *282*, 1823.

(13) Goyer, R. A.; Klaassen, C. D.; Waalkes, M. P. *Metal Toxicology*; Academic Press: New York, 1995.

(14) Pattison, D. I.; Davies, M. J.; Levina, A.; Dixon, N. E.; Lay, P. A. *Chem. Res. Toxicol.* **2001**, *14*, 500.

(15) Arfsten, D. P.; Aylward, L. L.; Karch, N. J. Chromium. In *Immunotoxicology of Environmental and Occupational Metals*; Zelikoff, J. T., Thomas, P. T., Eds.; Taylor & Francis Inc.: Bristol, PA, 1998.

(16) Chromium. In *National Research Council (US): committee on biologic effects of atmospheric pollutants*; National Academy of Sciences: Washington, DC, 1974; p 125.

(17) Adriano, D. C. *Trace Elements in the Terrestrial Environment*; Springer-Verlag: New York, 1986.

(18) Riley, R. G.; Zachara, J. M.; Wobber, F. J. *Chemical contaminants on DOE lands and selection of contaminant mixtures for subsurface science research*; U.S. Department of Energy: Washington, DC, 1992.

(19) Spliethoff, H. M.; Hemond, H. F. *Environ. Sci. Technol.* **1996**, *30*, 121.

(20) Kaehkoennen, M. A.; Suominen, K. P.; Manninen, P. K.; Salkinoja-Salonen, M. S. *Environ. Sci. Technol.* **1998**, *32*, 1741.

(21) Abu-Saba, K. E.; Flegal, A. R. *Environ. Sci. Technol.* **1997**, *31*, 3455.
(22) van Malderen, H.; Hoornaert, S.; van Grieken, R. *Environ. Sci. Technol.* **1996**, *30*, 489.
(23) Wang, W.-X.; Griscom, S. B.; Fisher, N. S. *Environ. Sci. Technol.* **1997**, *31*, 603.
(24) Ellis, A. S.; Johnson, T. M.; Bullen, T. D. *Science* **2002**, *295*, 2060.
(25) Buonicore, A. J. *Cleanup Criteria for Contaminated Soil and Groundwater*; ASTM: West Conshohocken, PA, 1996.
(26) Weckhuysen, B. M.; Wachs, I. E.; Schoonheydt, R. A. *Chem. Rev.* **1996**, *96*, 3327.
(27) Bartlett, R. J. *Environ. Health Perspect.* **1991**, *92*, 17.
(28) Fendorf, S.; Eick, M. J.; Grossl, P.; Sparks, D. L. *Environ. Sci. Technol.* **1997**, *31*, 315.
(29) Helsen, L.; Van den Bulck, E. *Environ. Sci. Technol.* **2000**, *34*, 2931.
(30) Holman, H. Y. N.; Perry, D. L.; Martin, M. C.; Lamble, G. M.; McKinney, W. R.; Hunter-Cevera, J. C. *Geomicrobiol. J.* **1999**, *16*, 307.
(31) Kendelewicz, T.; Liu, P.; Doyle, C. S.; Brown, G. E.; Nelson, E. J.; Chambers, S. A. *Surface Sci.* **1999**, *424*, 219.
(32) Kendelewicz, T.; Liu, P.; Doyle, C. S.; Brown, G. E. *Surface Sci.* **2000**, *469*, 144.
(33) Nico, P. S.; Fendorf, S. E.; Lowney, Y. W.; Holm, S. E.; Ruby, M. V. *Environ. Sci. Technol.* **2004**, *38*, 5253.
(34) Peterson, M. L.; Brown, G. E.; Parks, G. A. *Colloids Surf. A-Physicochem. Eng. Aspects* **1996**, *107*, 77.
(35) Peterson, M. L.; Brown, G. E.; Parks, G. A.; Stein, C. L. *Geochim. Cosmochim. Acta* **1997**, *61*, 3399.
(36) Pratt, A. R.; Blowes, D. W.; Ptacek, C. J. *Environ. Sci. Technol.* **1997**, *31*, 2492.
(37) Rinehart, T. L.; Schulze, D. G.; Bricka, R. M.; Bajt, S.; Blatchley, E. R. *J. Hazardous Mater.* **1997**, *52*, 213.
(38) Zachara, J. M.; Girvin, D. C.; Schmidt, R. L.; Resch, C. T. *Environ. Sci. Technol.* **1987**, *21*, 1.
(39) Zachara, J.; Cowan, C. E.; Schmidt, R. L.; Ainsworth, C. C. *Clays Clay Min.* **1988**, *36*, 317.
(40) Deng, B.; Stone, A. T. *Environ. Sci. Technol.* **1996**, *30*, 463.
(41) Deng, B.; Stone, A. T. *Environ. Sci. Technol.* **1996**, *30*, 2484.
(42) Buerge, I. J.; Hug, S. J. *Environ. Sci. Technol.* **1999**, *33*, 4285.
(43) Understanding Variation in Partition Coefficient, Kd, Values: Introduction.; United States Environmental Protection Agency, 2003; www.epa.gov/radiation/cleanup/partition.htm.
(44) Understanding Variation in Partition Coefficient, Kd, Values: Appendix E, Partition Coefficients for Chromium (VI); United States Environmental Protection Agency, 2003; www.epa.gov/radiation/cleanup/partition.htm.
(45) Langmuir, D. *Aqueous Environmental Geochemistry*; Prentice-Hall: NJ, 1997.
(46) Adamson, A. W. *Physical Chemistry of Surfaces*, 5th ed.; John Wiley & Sons: New York, 1990.
(47) Lindqvist-Reis, P.; Munoz-Paez, A.; Diaz-Moreno, S.; Pattanaik, S.; Persson, I.; Sandstrom, M. *Inorg. Chem.* **1998**, *37*.
(48) Munoz-Paez, A.; Sanchez Marcos, E. *J. Am. Chem. Soc.* **1992**, *114*, 6931.
(49) Diaz-Moreno, S.; Munoz-Paez, A.; Martinez, J. M.; Pappalardo, R. R.; Sanchez Marcos, E. *J. Am. Chem. Soc.* **1996**, *118*, 12654.
(50) Baron, D.; Palmer, C. D.; Stanley, J. T. *Environ. Sci. Technol.* **1996**, *30*, 964.
(51) Fitts, J. P.; Brown, G. E.; Parks, G. A. *Environ. Sci. Technol.* **2000**, *34*, 5122.
(52) Grossl, P. R.; Eick, M.; Sparks, D. L.; Goldberg, S.; Ainsworth, C. C. *Environ. Sci. Technol.* **1997**, *31*, 32.
(53) Peterson, M. L.; Brown, G. E.; Parks, G. A. In *Aqueous Chemistry and Geochemistry of Oxides, Oxyhydroxides, and Related Materials*; Voigt, J. A., Bunker, B. C., Casey, W. H., Wood, T. E., Crossey, L. J., Eds.; Materials Research Society: Pittsburgh, PA, 1997.
(54) Jardine, P. M.; Fendorf, S. E.; Mayes, M. A.; Larsen, I. L.; Brooks, S. C.; Bailey, W. B. *Environ. Sci. Technol.* **1999**, *33*, 2939.
(55) Weng, C. H.; Huang, C. P.; Allen, H. E.; Leavens, P. B.; Sanders, P. F. *Environ. Sci. Technol.* **1996**, *30*, 371.
(56) Rai, D.; Eary, L. E.; Zachara, J. M. *Sci. Total Environ.* **1989**, *86*, 15.
(57) Al-Abadleh, H. A.; Voges, A. B.; Bertin, P. A.; Nguyen, S. T.; Geiger, F. M. *J. Am. Chem. Soc.* **2004**, *126*, 11126.
(58) Voges, A. B.; Al-Abadleh, H. A.; Musorrafiti, M. J.; Bertin, P. A.; Nguyen, S. T.; Geiger, F. M. *J. Phys. Chem. B* **2004**, *108*, 18675.
(59) Konek, C. T.; Musorrafiti, M. J.; Al-Abadleh, H. A.; Bertin, P. A.; Nguyen, S. T.; Geiger, F. M. *J. Am. Chem. Soc.* **2004**, *126*, 11754.
(60) Al-Abadleh, H. A.; Mifflin, A. L.; Bertin, P. A.; Nguyen, S. T.; Geiger, F. M. *J. Phys. Chem. B* **2005**, *109*, 9691.
(61) Masel, R. I. *Principles of adsorption and reaction on solid surfaces*; John Wiley & Sons: New York, 1996.
(62) Strawn, D. G.; Sparks, D. L. *Soil Sci. Soc. Am. J.* **2000**, *64*, 144.
(63) Eisenthal, K. B. *Chem. Rev.* **1996**, *96*, 1343.
(64) Shen, Y. R. *The Principles of Nonlinear Optics*; John Wiley & Sons: New York, 1984.
(65) Heinz, T. F. *Nonlinear Surface Electromagnetic Phenomena*; Elsevier Publishers: Amsterdam, The Netherlands, 1991.
(66) Stack, A. G.; Higgins, S. R.; Eggleston, C. M. *Geochim. Cosmochim. Acta* **2001**, *65*, 3055.
(67) Fitts, J. P.; Shang, X.; Flynn, G. W.; Heinz, T. F.; Eisenthal, K. B. *J. Phys. Chem. B* **2005**, *109*, 7981.
(68) Yan, E. C. Y.; Eisenthal, K. B. *J. Phys. Chem. B* **1999**, *103*, 6056.
(69) Liu, Y.; Dadap, J. I.; Zimdars, D.; Eisenthal, K. B. *J. Phys. Chem. B* **1999**, *103*, 2480.
(70) Baldelli, S.; Schnitzer, C.; Campbell, D. J.; Shultz, M. J. *J. Phys. Chem. B* **1999**, *103*, 2789.
(71) Allen, H. C.; Gragson, D. E.; Richmond, G. L. *J. Phys. Chem. B* **1999**, *103*, 660.
(72) Wei, X.; Miranda, P. B.; Shen, Y. R. *Phys. Rev. Lett.* **2001**, *86*, 1554.
(73) Steel, W. H.; Damkaci, F.; Nolan, R.; Walker, R. A. *J. Am. Chem. Soc.* **2002**, *124*, 4824.
(74) Walker, R. A.; Conboy, J. C.; Richmond, G. L. *Langmuir* **1997**, *13*, 3070.
(75) Walker, R. A.; Gruetzmacher, J. A.; Richmond, G. L. *J. Am. Chem. Soc.* **1998**, *120*, 6991.
(76) Walker, R. A.; Smiley, B. L.; Richmond, G. L. *Spectroscopy* **1999**, *14*, 18.
(77) Richter, L. J.; Petralli-Mallow, T. P.; Stephenson, J. C. *Opt. Lett.* **1998**, *23*, 1594.
(78) Zhang, X.; Esenturk, O.; Walker, R. A. *J. Am. Chem. Soc.* **2001**, *123*, 10768.
(79) Zhang, X. C.; Walker, R. A. *Langmuir* **2001**, *17*, 4486.
(80) Voges, A. B.; Al-Abadleh, H. A.; Geiger, F. M. Development of Nonlinear Optical Spectroscopies for Studying Heterogeneous Environmental Catalytic Processes. In *Environmental Catalysis*; Grassian, V. H., Ed.; CRC Press: Boca Raton, FL, 2005.
(81) Geiger, F. M.; Pibel, C. D.; Hicks, J. M. *J. Phys. Chem. A* **2001**, *105*, 4940.
(82) Geiger, F. M.; Tridico, A. C.; Hicks, J. M. *J. Phys. Chem. B* **1999**, *103*, 8205.
(83) Mifflin, A. L.; Gerth, K. A.; Weiss, B. M.; Geiger, F. M. *J. Phys. Chem. A* **2003**, *107*, 6212.
(84) Mifflin, A. L.; Gerth, K. A.; Geiger, F. M. *J. Phys. Chem. A* **2003**, *107*, 9620.
(85) Simpson, G. Personal Communication; Purdue University, 2005.
(86) Steinfeld, J. I.; Francisco, J. S.; Hase, W. L. Chemical Kinetics and Dynamics, 2nd ed.; Prentice Hall: New York, 1999.
(87) Atkins, P. W. *Physical Chemistry*, 6th ed.; Oxford University Press: New York, 1998.
(88) Atkins, P. W. *Molecular Quantum Mechanics*; Oxford University Press: New York, 1983.
(89) Steinfeld, J. I.; Francisco, J. S.; Hase, W. L. *Chemical Kinetics and Dynamics*; Prentice Hall: Englewood Cliffs, NJ, 1989.
(90) Blowes, D. W.; Ptacek, C. J.; Jambor, J. L. *Environ. Sci. Technol.* **1997**, *31*, 3348.
(91) Su, C.; Puls, R. W. *Environ. Sci. Technol.* **2001**, *35*, 4562.